Elastic instability of polymer-shelled bubbles formed from air-in-oil-in-water compound bubbles†

Myung Han Lee and Daeyeon Lee*

Received 28th May 2010, Accepted 9th July 2010
DOI: 10.1039/c0sm00449a

We study the stability of polymer-shelled bubbles with controlled dimensions generated from air-in-oil-in-water (A/O/W) compound bubbles. We show that the ratio of the shell thickness to bubble radius is critical in generating un-deformed polymer-shelled bubbles from A/O/W compound bubbles. In addition, the effects of shell stiffness and encapsulated gas on bubble stability are also investigated.

A bubble is a globular body of gas suspended in a liquid. Monodisperse and stable bubbles have potential applications in food and cosmetics industries as well as in the fabrication of acoustic bandgap materials and functional lightweight materials with a hierarchical order.[1] Stable and monodisperse bubbles also can be advantageous in biomedical applications such as contrast-enhanced ultrasonography and ultrasound-triggered drug/gene delivery.[2] It is, however, challenging to make gas bubbles with controlled properties and narrow size distribution using traditional bubble generation methods, which typically rely on shearing gas in water.[3] In addition, bubbles in a liquid medium tend to dissolve and coarsen over a period of time due to the Laplace pressure across the air–water interface, limiting their long-term utilization.[4,5]

Recently, bubbles with extended lifetime have been generated by covering the bubbles with different materials. Bubbles coated with insoluble surfactants, phospholipids or biopolymers have been reported to have significantly enhanced stability against dissolution.[5,6] Bubbles stabilized by colloidal particles, referred to as "armored bubbles", also are extremely stable due to the presence of a stiff interfacial layer that arrests bubble dissolution.[7,8] From these studies, it is evident that the physicochemical properties of the bubble shell formed at the gas–liquid interface are critical in suppressing bubble dissolution, coalescence, and coarsening. Although the effect of the chemical properties of shell materials has been studied previously, the effects of shell thickness and stiffness on the stability of bubbles have not been investigated extensively. The lack of such investigation is partly attributed to the significant difficulties involved in generating bubbles with controlled dimensions such as radius and shell thickness.

We have recently reported a new approach to generate monodisperse and stable bubbles with a stiff shell of randomly packed nanoparticles by employing an air-in-oil-in-water (A/O/W) compound bubble as a template.[9] Our approach affords precise control over bubble dimensions (*i.e.*, radius and shell thickness) and also allows for the incorporation of non-water soluble materials such as hydrophobic polymers and nanoparticles, thereby enhancing the potential utility of bubbles in various applications. In this work, we study the effects of bubble dimension, shell material, and encapsulated gas on the stability of polymer-shelled bubbles generated from an A/O/W compound bubble.

Polymer-shelled bubbles using a glassy biocompatible polymer, poly(DL-lactic-*co*-glycolic)acid (PLGA), are created using an A/O/W compound bubble as a template, as shown in Fig. 1(a).[9] The monodisperse A/O/W compound bubble is generated using a glass capillary microfluidic device (Fig. 1(b)). The inner phase (A) is nitrogen, and the outer phase (W) is a mixture of glycerol and 2 wt% poly(vinyl alcohol) (PVA) aqueous solution. The middle phase (O) comprises a volatile organic solvent, dichloromethane, in which PLGA is dissolved. Inner and middle fluid streams are hydrodynamically focused by the outer fluid, leading to the formation of compound bubbles with a polydispersity of less than 7%. Polymer-shelled bubbles are obtained by removing the solvent *via* evaporation. This method of polymer-shelled bubble generation enables us to precisely control the bubble radius (R) and the thickness of the bubble shell (h).

Upon solvent removal, we observe that some polymer-shelled bubbles undergo deformation, exhibiting buckling or irreversible change in the shape of shells as seen in Fig. 1(c). Other bubbles with different dimensions, however, show little deformation as shown in Fig. 1(d). To characterize the effect of bubble dimension on the bubble deformation, we determine the percentage of deformed bubbles as functions of shell thickness (h) and bubble radius (R), as illustrated in a state diagram (Fig. 2). For a given bubble radius, an increase in shell thickness leads to an increase in the fraction of un-deformed bubbles, whereas for a given shell thickness, an increase in bubble size leads to a decrease in bubble stability as shown in Fig. 2. This observation clearly indicates that the deformation of bubble shell is strongly influenced by the combined effect of the shell thickness and bubble radius.

The stability of the bubble shell is seen to correlate strongly with the ratio of shell thickness to bubble radius, h/R, as shown in Fig. 3. As h/R increases, the percentage of deformed bubbles decreases, reflecting an increase in the bubble stability against deformation. The fraction of un-deformed bubble plateaus as h/R is increased above a critical value. Consequently, the critical ratio of bubble shell

Department of Chemical and Biomolecular Engineering, University of Pennsylvania, Philadelphia, PA, 19104, USA. E-mail: daeyeon@seas.upenn.edu; Fax: (+215) 573-2093; Tel: (+215) 573-4521

† Electronic supplementary information (ESI) available: (1) the calculation of shell thickness (h) and bubble size (R) from the optical microscopy images of compound bubbles generated in a microfluidic device, (2) optical microscopy images showing the droplets of polymer-oil solution shrink isotropically without the formation of an elastic boundary layer during the solvent removal process, (3) percentage of deformed bubbles for different shell materials and filling gases as a function of h/R at 30 min, (4) optical microscopy image of a buckled film in water, and (5) images of bubble shape based on the value of the calculated eccentricity. See DOI: 10.1039/c0sm00449a

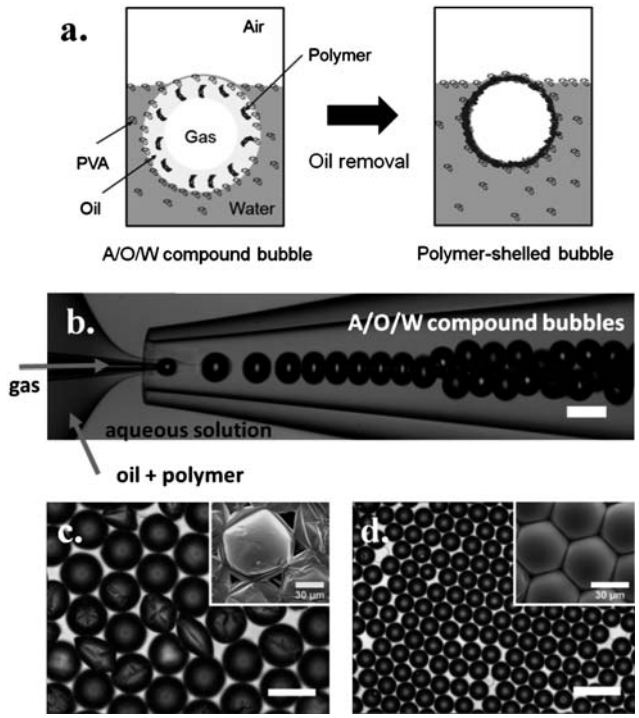

Fig. 1 Microfluidic fabrication of PLGA-shelled bubbles. (a) Schematic for the formation of polymer-shelled bubbles from A/O/W compound bubbles. (b) Optical microscopy image of A/O/W compound bubbles generated in a microfluidic device. (c,d) Optical microscopy images of PLGA-shelled bubbles 30 min after preparation. Bubbles have (c) $R =$ 40.9 μm and $h = 104$ nm and (d) $R = 19.3$ μm and $h = 93$ nm. We note that R and h are determined by the mass balance using oil flow rate (Q_m), compound-bubble generation frequency (f_{cb}), volume fraction of polymer in oil (ϕ_p), and compound-bubble size (D_{cb}) (see ESI for the calculation of R and h). Insets show the SEM images of polymer shells after being completely air-dried at room temperature. Scale bars are 100 μm.

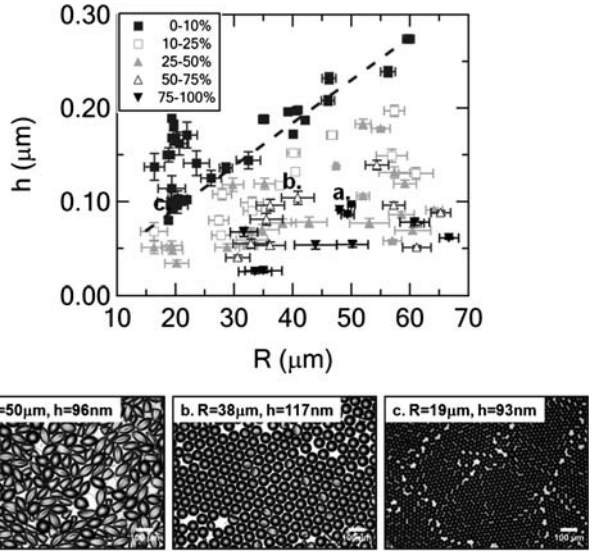

Fig. 2 State diagram for bubble stability as functions of the shell thickness (h) and bubble radius (R), determined at 30 min after preparation. The symbols depend on the percentage of deformed bubbles: (■) 0–10%; (□) 10–25%; (▲) 25–50%; (△) 50–75%; (▼) 75–100%. The dashed line goes through the origin of the h versus R graph and has a slope of $(h/R)_c$. Optical microscopy images correspond to the several data points (a, b and c) on the diagram.

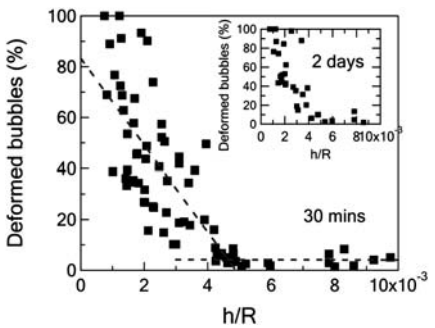

Fig. 3 Percentage of deformed bubbles as a function of h/R at 30 min after preparation and (inset) 2 days after preparation.

thickness to bubble radius, $(h/R)_c$, for the onset of bubble shell deformation is determined to be 0.0046. The stable–unstable transition of bubble shell can be clearly delineated by a line with a slope of $(h/R)_c$ as seen in Fig. 2 (this line goes through the origin of the plot). We note that there is no significant change in the fraction of deformed bubbles two days after preparation as shown in Fig. 3. The onset of bubble instability occurs within 30 min after preparation.

We believe the deformation of bubble shell is due to the partitioning of gas (*i.e.*, nitrogen) into the surrounding aqueous phase and the air above the aqueous phase by its diffusion through the elastic polymer shell that has formed after the solvent removal.[10] The diffusion of gas through the elastic polymer shell leads to a pressure difference. The pressure difference, thus, will depend on the difference in the chemical potential of the gaseous species across the bubble shell but not strongly on the bubble dimension and the shell material. The pressure difference that induces shell deformation can be expressed using the following equation describing the elastic instability of a spherical shell[11]

$$\Delta P = \frac{2E_f}{\sqrt{3(1-\nu^2)}}\left(\frac{h}{R}\right)_c^2 \quad (1)$$

where ν and E_f are the Poisson's ratio and Young's modulus of the bubble shell.

We hypothesize that different filling gases would lead to different values of ΔP. To confirm this, we generate PLGA-shelled bubbles using different gases. The values of ΔP are determined to be a strong function of the identity of filling gas as summarized in Table 1. While the generation of bubbles using compressed air leads to a smaller value of ΔP compared to N_2-filled bubbles, the bubbles generated using helium (He) and carbon dioxide (CO_2)[8,12] exhibit higher values of ΔP compared to N_2-filled bubbles. The fact that the bubbles filled with He, which has a low solubility in water,[13] have a higher value of ΔP than N_2-filled bubbles indicates that it is not just the solubility of gas in water but also its transfer into the air above water that determine the pressure difference. Because of the scarcity of He in air, the pressure difference for He-filled bubbles is greater than that of N_2-filled bubbles. Thus, our results indicate that the partitioning of filling gas in the air above water surface as well as the solubility of gas in the surrounding water are critical in determining the pressure difference across the bubble shells.

Table 1 The pressure difference across the polymer shell determined by the critical h/R and Young's moduli E_f. Young's moduli of polymer films immersed in water for 30 min are measured using a buckling-based metrology

Shell	Gas	$(h/R)_c$	E_f (GPa)	ΔP (kPa)
PLGA	N_2	0.0046	1.69 ± 0.54	43.8 ± 14.1
	Air	0.0038		29.9 ± 9.6
	CO_2	0.0068		95.8 ± 30.7
	He	0.0054		60.4 ± 19.4
PS	N_2	0.0035	3.06 ± 0.36	45.8 ± 5.5
PMMA	N_2	0.0040	2.25 ± 0.30	44.0 ± 5.9

The pressure difference (ΔP) that leads to the deformation of polymer-shelled bubbles can be determined by measuring the Young's modulus of the polymer (E_f) as well as the critical ratio of shell thickness to bubble radius, $(h/R)_c$. As indicated above, ΔP should not depend on the properties of the shell material but rather on the identity of filling gas. To confirm this hypothesis, we determine the pressure difference inducing the deformation of nitrogen-filled bubbles by generating bubbles with different shell materials (Table 1). Glassy polymers, poly(methyl methacrylate) (PMMA) and polystyrene (PS), are used to determine the pressure difference across the bubble shell. The critical ratio $(h/R)_c$ for each polymer is determined using the method described above (see ESI, Figure S2). The Young's modulus (E_f) of each polymer in water is determined using a strain-induced elastic buckling instability for mechanical measurement (SIEBIMM) method[14,15] (see Experimental section and ESI for details (Figure S3)). The pressure differences (ΔP) for N_2-filled bubbles obtained using the three different polymers are in an excellent agreement with each other as summarized in Table 1. The consistency obtained from N_2-filled bubbles generated with the three polymers clearly indicates that ΔP depends on the identity of the filling gas rather than on the shell material and bubble size. We note that the bubble shell may have a small amount of residual solvent, which would lead to the overestimation of E_f as well as ΔP.[16]

From these results, we can conclude that gases that have a high solubility in water and are rare in air tend to increase the value of $(h/R)_c$. Thicker polymer shells are required to generate un-deformed bubbles when these types of gases are used for bubble generation. Also, the stiffer polymer shell requires a smaller value of $(h/R)_c$ to generate un-deformed bubbles; that is, un-deformed bubbles can be generated more easily with thinner shells for a given bubble radius if stiffer polymers are used.

Eqn (1) also suggests that a universal behavior may exist. It can be deduced that the deformation behavior of bubbles generated with different shell materials but with a given filling gas would scale as $E_f(h/R)^2$. When the fraction of deformed bubbles (N_2-filled) for each polymer (Fig. 4(a)) is scaled accordingly, the three curves superpose reasonably well onto a single master curve (Fig. 4(b)), indicating, indeed, the instability of polymer-shelled bubbles is a consequence of pressure difference induced by gas diffusion from the inside of the bubbles to the outside through the elastic polymer shell.

In summary, we investigated the elastic instability of polymer-shelled bubbles produced from A/O/W compound bubbles. The microfluidic technique provides a unique opportunity in creating bubbles with precisely controlled dimensions and, thus, we can investigate the effect of shell thickness and radius on the stability of bubble with unprecedented control. We found that the ratio of shell thickness to bubble radius plays a critical role in determining the bubble stability against deformation. In addition, the pressure difference (ΔP) across bubble shell at the onset of shell deformation was determined by measuring the critical ratio of shell thickness to bubble radius, $(h/R)_c$. The pressure difference was found to be strongly dependent on the identity of the encapsulated gas, which indicates that ΔP is mainly determined by gas dissolution into the surrounding liquid and the air above the liquid. The use of a gas that is highly soluble in water and scarce in air (*e.g.*, CO_2), thus, leads to the elastic instability of bubbles against deformation. In addition, the use of stiff polymer shells enables the generation of un-deformed bubbles with small values of h/R. Our results provide guidance for the generation of stable bubbles with controlled physical properties for future applications in the generation of three-dimensional porous materials.

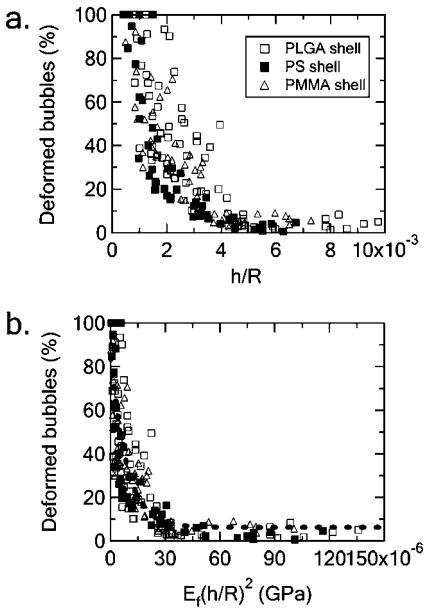

Fig. 4 Percentage of deformed bubbles with the PLGA-, PS-, and PMMA-shells as a function of (a) h/R and (b) $E_f(h/R)^2$.

Experimental

Preparation of polymer-shelled bubbles

The A/O/W compound bubbles are generated using a glass-capillary microfluidic device that combines a co-flow and flow-focusing geometry, as described previously.[9] Briefly, two circular capillary tubes with inner and outer diameters of 0.58 mm and 1.0 mm (World Precision Instrument Inc.) were tapered to desired diameters using a micropipette puller (P-1000, Sutter Instrument Inc.) and a microforge (Narishige MF-830). The inner diameters of tapered tubes for the injection of a gas phase and the collection of bubbles were 2–8 μm and 80–150 μm, respectively. The outside of the glass capillary tube for inner fluid was hydrophobically functionalized with octadecyltrichlorosilane (OTS). This chemical treatment enhances the wettability of oil outside the capillary tube, and facilitates the formation of compound bubbles. The two tapered capillaries were inserted into a square capillary with an inner dimension of 1.0 mm, and subsequently sealed with epoxy.

For the fabrication of compound bubbles, one gas and two liquids were introduced into a microfluidic device using flexible Tygon tubing with a pressure regulator (ControlAir Inc.) and two syringe pumps (PHD, Harvard Apparatus), respectively. The inner gas phase was nitrogen (N_2), compressed air, carbon dioxide (CO_2), or helium (He), and the middle oil phase consisted of 1–5 wt% PLGA polymer (75 : 25 poly(DL-lactic-*co*-glycolic)acid, Ester Terminated, Durect Corp.) in dichloromethane. The outer water phase was composed of a mixture of 0–50 vol% glycerol in 2 wt% PVA aqueous solution (PVA, 87–89% hydrolyzed, average M_w = 13 000–23 000, Aldrich). The increase in viscosity using glycerol enables the generation of compound bubbles with relatively low flow-rate of outer phase. The compound-bubble generation frequency (f_{cb}) was measured for calculating bubble dimensions such as shell thickness and bubble radius (see ESI for details). Generated compound bubbles flowed into the collection tube, and then one or two drops containing compound bubbles were collected into a large pool of water on a glass slide. This effectively lowers the concentration of PVA and glycerol in the continuous phase. The collected bubbles formed a monolayer at the top of water surface on the glass slide. The organic solvent was removed simply *via* evaporation. Because the bubbles float to the water surface, the evaporation of the solvent occurs very rapidly. Based on the evaporation rate of the solvent, we expect the solvent to be removed in approximately 30 s. For the generation of PS- and PMMA-shelled bubbles, the middle phases were prepared by dissolving 2–4 wt% PS (M_w = 400 000, $M_w/M_n \leq 1.06$, Pressure Chemical Co.) and 2–6 wt% PMMA (M_w = 75 000, Scientific Polymer Products Inc.) in toluene, respectively.

The generation of compound bubbles in a device was monitored with a 10× objective using an inverted light microscope (Nikon Diaphot 300) equipped with a high-speed camera (Phantom V7.1) capable of 13 000 frames per second at the frame resolution of 800 × 200 pixels. The polymer-shelled bubbles formed from compound bubbles were imaged using an upright microscope (Carl Zeiss Axio Plan II) with a CCD camera (Qimaging Retiga 2000R Fast 1394). The percentage of deformed bubbles was determined by measuring the eccentricity of at least 250 bubbles using the ImageJ software and counting the number of particles below the eccentricity-threshold of 0.85 (see ESI for bubble shape based on the calculated eccentricity, Figure S4). The scanning electron microscope (SEM) images were taken using a Quanta 600 FEG Mark II at an acceleration voltage of 5kV.

Young's modulus measurements

Young's modulus of the polymer film in water was measured *via* strain-induced elastic buckling instability for mechanical measurement (SIEBIMM) method.[14,15] This method determines the Young's modulus of polymer thin films based on their buckling on polydimethylsiloxane (PDMS) elastomer substrate induced by a uniaxial compression. To prepare the samples for testing, polymer films were transferred from silicon wafers onto PDMS substrates, as described previously.[14,15] Briefly, PDMS substrates (Sylgard 184, Dow Corning) were prepared by curing the degassed pre-polymer and initiator in a 10 : 1 w/w ratio for 2 h at 75 °C. Thin films of polymers were spin-coated from toluene solutions of PS and PMMA and chloroform solutions of PLGA onto plasma-treated silicon wafers. In the case of PLGA, films were deposited onto polyacrylic acid (PAA, 35 wt% aqueous solution, M_w = 100,000, Sigma-Aldrich)-coated silicon wafers because of the difficulty in directly transferring the relatively hydrophilic polymer film to the PDMS substrate in water. The PAA dissolved in water releasing the polymer film readily from the silicon wafer.

The polymer films on the PDMS substrates were buckled under water by applying a compressive strain using a pair of tweezers under a Nikon Diaphot 300 inverted microscope. The polymer films were left in water for at least 30 min. The wavelength of the buckling patterns was measured using a fast Fourier transform (FFT) of the optical image (see ESI for an optical microscope image, Figure S3). The thickness of polymer films on the OTS-coated silicon-wafer in water was measured using an alpha-SE spectroscopic ellipsometer (J. W. Woollam Co., Inc.) with a home-made liquid cell. The OTS-layer prevents the delamination of the polymer film from Si wafers under water. With the measured values of buckling wavelength λ and film thickness h_{film}, the Young's modulus of polymer film was calculated using this equation[15]

$$E_f = \frac{3E_s\left(1-\nu_f^2\right)}{1-\nu_s^2}\left(\frac{\lambda}{2\pi h_{film}}\right)^3, \quad (2)$$

where subscripts f and s indicate the polymer film and PDMS substrate, respectively, as shown in Table 1. The Young's modulus of PDMS (E_s) was independently measured using a dynamic mechanical analyzer (DMA; Q800 TA Instruments). Poisson's ratios of 0.33 and 0.5 were used for polymer and PDMS, respectively.[14,17]

Acknowledgements

This work was supported by the PENN MRSEC DMR-0520020, and partly by the Nano/Bio Interface Center (NBIC) through the National Science Foundation NSEC DMR-0425780, the University Research Foundation of the University of Pennsylvania, and Amore-Pacific Co. We thank Professor Russell Composto of University of Pennsylvania for the use of a spin-coater and the provision of polystyrene, and thank Professor John Bassani of University of Pennsylvania for helpful discussions regarding the mechanical response of shells. We also thank Professor Adam J. Nolte of Rose-Hulman Institute of Technology for valuable discussions regarding the SIEBIMM technique, and Jamie Ifkovits, Elena Tous, and Professor Jason Burdick of University of Pennsylvania for the measurements of the modulus of PDMS. We thank Jennifer Kay of the University of Pittsburg for her preliminary studies on the polymer-shelled bubble generation.

Notes and references

1 B. P. Binks and R. Murakami, *Nat. Mater.*, 2006, **5**, 865–869; R. G. Alargova, D. S. Warhadpande, V. N. Paunov and O. D. Velev, *Langmuir*, 2004, **20**, 10371–10374; V. Leroy, A. Strybulevych, J. H. Page and M. G. Scanlon, *J. Acoust. Soc. Am.*, 2008, **123**, 1931–1940.
2 E. C. Unger, T. O. Matsunaga, T. McCreery, P. Schumann, R. Sweitzer and R. Quigley, *Eur. J. Radiol.*, 2002, **42**, 160–168; K. Ferrara, R. Pollard and M. Borden, *Annu. Rev. Biomed. Eng.*, 2007, **9**, 415–447.
3 K. P. Pancholi, U. Farook, R. Moaleji, E. Stride and M. J. Edirisinghe, *Eur. Biophys. J. Biophys. Lett.*, 2008, **37**, 515–520; E. Stride and M. Edirisinghe, *Soft Matter*, 2008, **4**, 2350–2359.
4 A. Dutta, A. Chengara, A. D. Nikolov, D. T. Wasan, K. Chen and B. Campbell, *J. Food Eng.*, 2004, **62**, 177–184.
5 M. A. Borden and M. L. Longo, *Langmuir*, 2002, **18**, 9225–9233.

6 J. Il Park, E. Tumarkin and E. Kumacheva, *Macromol. Rapid Commun.*, 2010, **31**, 222–227; E. Dressaire, R. Bee, D. C. Bell, A. Lips and H. A. Stone, *Science*, 2008, **320**, 1198–1201; E. Talu, M. M. Lozano, R. L. Powell, P. A. Dayton and M. L. Longo, *Langmuir*, 2006, **22**, 9487–9490.
7 M. Abkarian, A. B. Subramaniam, S. H. Kim, R. J. Larsen, S. M. Yang and H. A. Stone, *Phys. Rev. Lett.*, 2007, **99**, 188301; A. B. Subramaniam, M. Abkarian, L. Mahadevan and H. A. Stone, *Nature*, 2005, **438**, 930–930.
8 J. I. Park, Z. Nie, A. Kumachev, A. I. Abdelrahman, B. R. Binks, H. A. Stone and E. Kumacheva, *Angew. Chem., Int. Ed.*, 2009, **48**, 5300–5304.
9 M. H. Lee, V. Prasad and D. Lee, *Langmuir*, 2010, **26**, 2227–2230.
10 The evaporation of solvent from the oil layer could, in principle, lead to buckling due to the formation of an elastic layer at the oil–water interface (N. Tsapis, E. R. Dufresne, S. S. Sinha, C. S. Riera, J. W. Hutchinson, L. Mahadevan and D. A. Weitz, *Phys. Rev. Lett.*, 2005, **94**, 018302). However, we believe that the deformation of the bubble shell is not induced by the buckling of the stiff polymer layer that could form at the oil–water interface during the solvent removal process. Our experiment using single emulsions of polymer solution does not indicate that the evaporation of solvent leads to buckling of droplets during solvent removal (see ESI for optical microscopy images, Fig. S1).
11 D. Landau and E. M. Lifshitz, *Theory of Elasticity*, London, Pergamon Press; Reading, Mass., Addison-Wesley Pub. Co., 1959.
12 J. I. Park, Z. H. Nie, A. Kumachev and E. Kumacheva, *Soft Matter*, 2010, **6**, 630–634.
13 V. B. Konstantinov, A. F. Malyi and V. A. Babenko, *Tech. Phys. Lett.*, 2003, **29**, 566–568.
14 A. J. Nolte, N. D. Treat, R. E. Cohen and M. F. Rubner, *Macromolecules*, 2008, **41**, 5793–5798.
15 C. M. Stafford, C. Harrison, K. L. Beers, A. Karim, E. J. Amis, M. R. Vanlandingham, H. C. Kim, W. Volksen, R. D. Miller and E. E. Simonyi, *Nat. Mater.*, 2004, **3**, 545–550.
16 E. Lorenceau, A. S. Utada, D. R. Link, G. Cristobal, M. Joanicot and D. A. Weitz, *Langmuir*, 2005, **21**, 9183–9186.
17 A. J. Nolte, Ph.D. Thesis, Massachusetts Institute of Technology, 2007.

